Since January 2020 Elsevier has created a COVID-19 resource centre with free information in English and Mandarin on the novel coronavirus COVID-19. The COVID-19 resource centre is hosted on Elsevier Connect, the company's public news and information website.

Bioorganic Chemistry 135 (2023) 106527

Contents lists available at ScienceDirect

Bioorganic Chemistry

journal homepage: www.elsevier.com/locate/bioorg

Synthesis and anti-SARS-CoV-2 evaluation of lipid prodrugs of β-D-N^4-hydroxycytidine (NHC) and a 3′-fluoro-substituted analogue of NHC

Zhao-Hui Wen [a,1], Meng-Meng Wang [b,1], Ling-Yun Li [a], Piet Herdewijn [c], Robert Snoeck [d], Graciela Andrei [d,*], Zhao-Peng Liu [a,*], Chao Liu [a,*]

[a] Department of Medicinal Chemistry, Key Laboratory of Chemical Biology (Ministry of Education), School of Pharmaceutical Sciences, Cheeloo College of Medicine, Shandong University, Jinan 250012, China
[b] Biology Institute, Qilu University of Technology (Shandong Academy of Sciences), Jinan 250103, China
[c] Medicinal Chemistry, Rega Institute for Medical Research, KU Leuven, 3000 Leuven, Belgium
[d] Laboratory of Virology and Chemotherapy, Rega Institute for Medical Research, KU Leuven, 3000 Leuven, Belgium

ARTICLE INFO

Keywords:
Nucleoside analogue
SARS-CoV-2
COVID-19
EIDD-1931
Lipid prodrugs

ABSTRACT

β-D-N^4-hydroxycytidine (NHC, EIDD-1931) is a nucleoside analogue that exhibits broad spectrum antiviral activity against a variety of RNA viruses. Herein, we report the synthesis of a series of lipid prodrugs of NHC and a novel 3′-fluoro modified NHC analogue, and evaluation of their antiviral activity against five variants of SARS-CoV-2. All lipid prodrugs showed potent antiviral activity against the tested SARS-CoV-2 variants with EC_{50} values in the range of 0.31–3.51 μM, which were comparable to those of NHC or higher than those of remdesivir and molnupiravir. An increase in the cytostatic activity of the lipid prodrugs was found, but prodrug **2d** proved equally selective as molnupinavir. The 3′-F analogue of NHC (**6**) only displayed minor antiviral activity against the SARS-CoV-2 Omicron variant (EC_{50} = 29.91 μM), while no activity was found for other variants at the highest concentration tested. The promising antiviral data of the lipid prodrugs of NHC suggest that they deserve further investigation as new anti-SARS-CoV-2 drugs.

1. Introduction

The global coronavirus disease 2019 (COVID-19) pandemic caused by severe acute respiratory syndrome coronavirus 2 (SARS-CoV-2) has infected >700 million people and caused 6 million deaths worldwide as of February 2023 [1]. Despite the successful development of several antiviral drugs for treating COVID-19, there is still an unmet need for safe and effective antiviral drugs against SARS-CoV-2 and its variants of concern (VOC) [2–4]. Nucleoside/tide analogues (NAs) have long been used for the treatment of viral infections, and now present an important class of drugs in the fight against SARS-CoV-2. A number of NAs such as remdesivir, VV116, molnupiravir, azvudine and bemnifosbuvir (Fig. 1), have been approved or in clinical trial for the treatment of COVID-19 [5–9]. Remdesivir was the first antiviral treatment approved for COVID-19 by the United States Food and Drug Administration (FDA) [10]. However, it can only be administered intravenously and its use is extremely limited. Molnupiravir (EIDD-2801), a newly repositioned synthetic nucleoside, was recently approved by the UK Medicines and Healthcare products Regulatory Agency (MHRA) for the treatment of mild to moderate COVID-19 patients, becoming the world's first oral anti-COVID-19 drug [11].

Molnupiravir is an isopropyl prodrug of β-D-N^4-hydroxycytidine (NHC; EIDD-1931) [12]. NHC has been reported to exhibit a broad-spectrum activity against a variety of RNA viruses, including chikungunya virus, Venezuelan equine encephalitis virus (VEEV), respiratory syncytial virus (RSV), hepatitis C virus (HCV), norovirus, influenza, Ebola virus (EBOV), SARS-CoV-2, MERS-CoV, SARS-CoV, and related zoonoses 2b or 2c bat coronaviruses [7–11]. Preclinical and clinical studies have shown that molnupiravir is effective for the treatment of SARS-CoV-2 infection with a favourable safety profile [11,13–16], although some concerns have been raised regarding the mutagenic potential of NHC [17]. After oral administration, molnupiravir is quickly cleaved in plasma to NHC, which after distribution into various tissues, is converted into its corresponding 5′-triphosphate by host kinases [18]. The active 5′-triphosphate serves as a competitive alternative substrate for viral RNA-dependent RNA polymerase (RdRp), upon incorporation

* Corresponding authors.
E-mail addresses: graciela.andrei@kuleuven.be (G. Andrei), liuzhaop@sdu.edu.cn (Z.-P. Liu), chaoliu@sdu.edu.cn (C. Liu).
[1] Zhao-Hui Wen and Meng-Meng Wang contributed equally to this work.

https://doi.org/10.1016/j.bioorg.2023.106527
Received 9 February 2023; Received in revised form 12 March 2023; Accepted 3 April 2023
Available online 6 April 2023

into nascent viral RNA chain, leads to the accumulation of mutations in the viral genome, resulting in lethal mutations [19,20]. The presence of the 3′-to-5′ exoribonuclease (ExoN) domain of coronaviruses poses a challenge for the treatment of COVID-19 with NAs. The proofreading exonuclease can excise incorporated nucleotide analogues and diminish their inhibitory effects, but NHC has been found to be resistant to this proofreading activity [20]. However, NHC demonstrated poor oral bioavailability in animal models. It was rapidly metabolized in the enterocytes of non-human primates after oral administration [21]. In addition, uptake of NHC from the plasma into tissues appears to be mediated by sodium-dependent concentrative transporters and high plasma levels of uridine can effectively outcompete the uptake and distribution of NHC [15]. Thus, it is interesting to develop prodrug forms of NHC to overcome these issues.

Previous studies have shown that certain fatty acyl conjugates of the anti-HIV nucleosides such as lamivudine (3TC), emtricitabine (FTC), and stavudine (d4T) exhibited enhanced activity against X4, R5, cell associated, and/or multi-drug resistant strains compared with their parent nucleosides [22–24]. For example, 5′-*O*-myristoyl and 5′-*O*-12-azidododecanoyl derivatives of 3TC displayed at least 16–36-fold higher anti-HIV activity against cell-free virus than 3TC [22]. 5′-*O*-myristoyl derivative of FTC exhibited 10–24-times higher anti-HIV activity than FTC alone [24]. Recently, EI-Sayed et al. reported that remdesivir can be modified with fatty acids such as myristic acid, 12-azidododecanoic, and palmitic acid without demonstrating a significant loss of antiviral activity in cell culture against SARS-CoV-2 and EBOV while generating long-acting effect in vitro [25]. Furthermore, the fatty acyl conjugates and other lipid prodrugs have also been reported to exhibit reduced toxicity, enhanced cellular uptake, improved lung exposure/selectivity and oral bioavailability compared to their parent nucleoside analogues [26–28].

Inspired by the potent antiviral activity of lipid prodrugs of antiviral nucleosides as well as their favourable pharmacokinetic properties, here, we report the synthesis of a series of lipid prodrugs of NHC and the evaluation of their antiviral activity against five variants of SARS-CoV-2 in Vero E6 cells. Four fatty acids, tetradecyl carbonate, palmitic acid, myristic acid, and lauric acid were conjugated to NHC at its N^4-hydroxy position. The fatty acid selection was based on the antiviral activity for the previously reported lipid prodrugs of NAs [22–25]. It was expected that the lipid prodrugs of NHC may have different physicochemical properties from molnupiravir, leading to improved antiviral activities and biological profiles [25–29]. In addition, in view of the proofreading exonuclease of coronaviruses can excise incorporated nucleotide analogues and diminish the inhibitory effects, to investigate the influence of 3′-hydroxy of NHC on anti-SARS-CoV-2 activity, a previously unknown 3′-deoxy-3′-fluoro modified NHC analogue was also prepared and evaluated.

2. Results and discussion

2.1. Synthesis of lipid prodrugs of NHC

The synthesis of N^4-hydroxycytidine lipid prodrugs **2a-d** is shown in Scheme 1. Four different fatty acids, tetradecyl carbonate, palmitic acid, myristic acid, and lauric acid, in the form of acyl chloride or chloroformate, underwent reaction with the N^4-hydroxyl group of NHC. The conjugation of the fatty acid to NHC was accomplished by reacting 1.1 M equivalents of the corresponding fatty acyl chloride or chloroformate with a dilute solution of NHC in dry pyridine to give mono-fatty acyl derivatives **2a-d** in 62–82% yield. The free N^4-hydroxy of NHC has been shown to be more reactive than the free 2′, 3′ and 5′-hydroxy groups [30]. The lipid prodrugs were fully characterized using nuclear magnetic resonance (NMR) and high-resolution mass spectroscopy (HRMS).

It is worth noting that the ^{1}H NMR of these prodrugs recorded in DMSO-d_6 showed several minor peaks accounting for 20–40% relative to the major peaks, though the RP-HPLC traces showed high purity of the compounds. This observation would be in line with literature reports for NHC and its N^4-hydroxy derivatives that the *N*-hydroxycytosine can exist as a tautomer of the amine and imine [30]. To investigate this possibility, a viable temperature (VT) NMR experiment was performed for compound **2a** in DMSO-d_6, increasing temperature at intervals of 10 up to 60 °C. At elevated temperatures, the intensity of the minor peak slightly decreased (Fig. 2). Furthermore, ^{1}H NMR spectra were recorded in protic solvent to disrupt hydrogen bonding and isomerization. As expected, the amount of the minor isomer was significantly decreased in MeOH-d_4 and the major isomer grew in intensity (Fig. 3). The above results indicate the existence of tautomers for the synthesized prodrugs.

The enhanced lipophilicity of these lipid prodrugs relative to NHC and its isopropyl prodrug molnupiravir was expected to increase their permeability properties to achieve a higher concentration of the

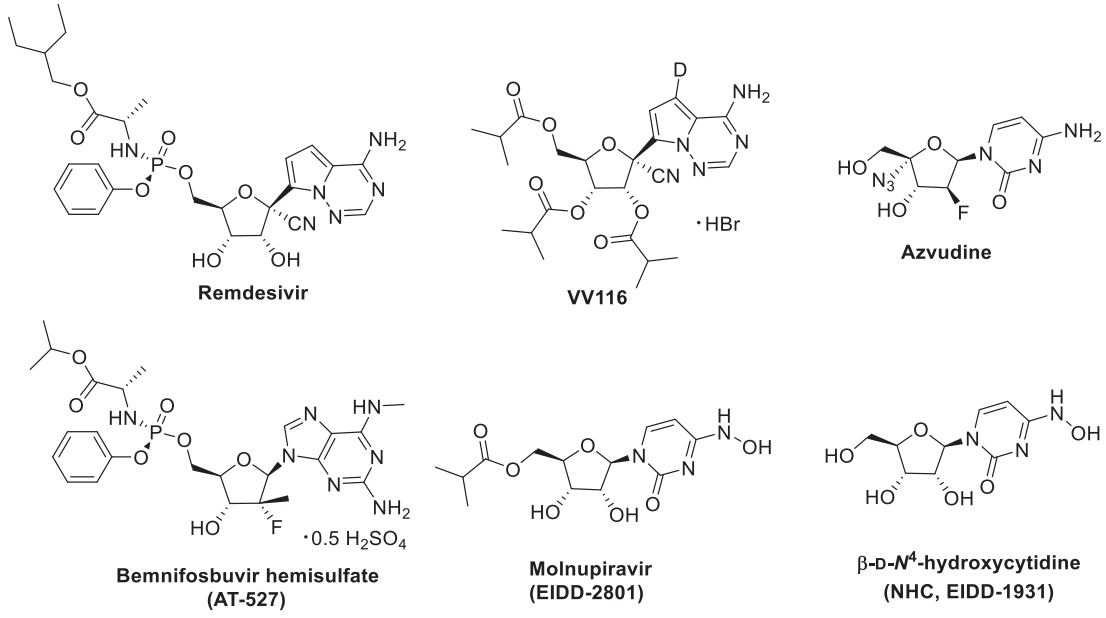

Fig. 1. Selected examples of biologically active nucleoside/tide anti-SARS-CoV-2 agents.

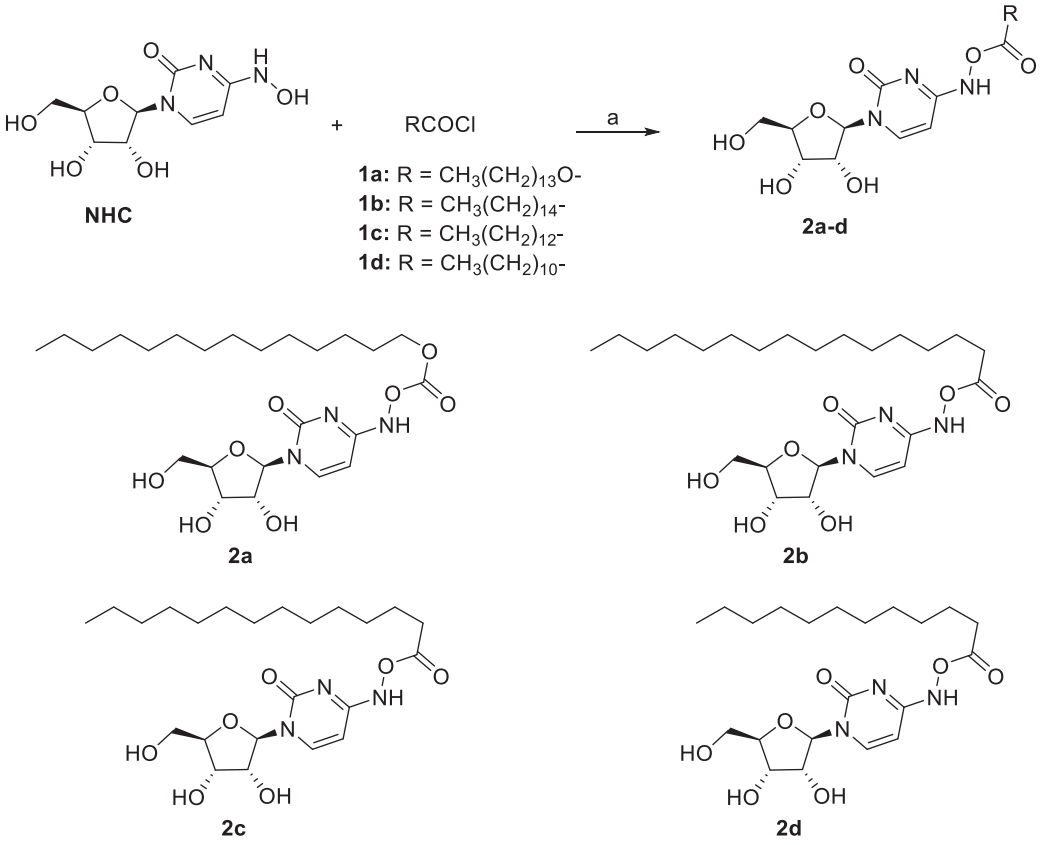

Scheme 1. Synthesis of lipid prodrugs of NHC. Reagents and conditions: (a) **1a-d**, pyridine, rt, overnight, 62–82%.

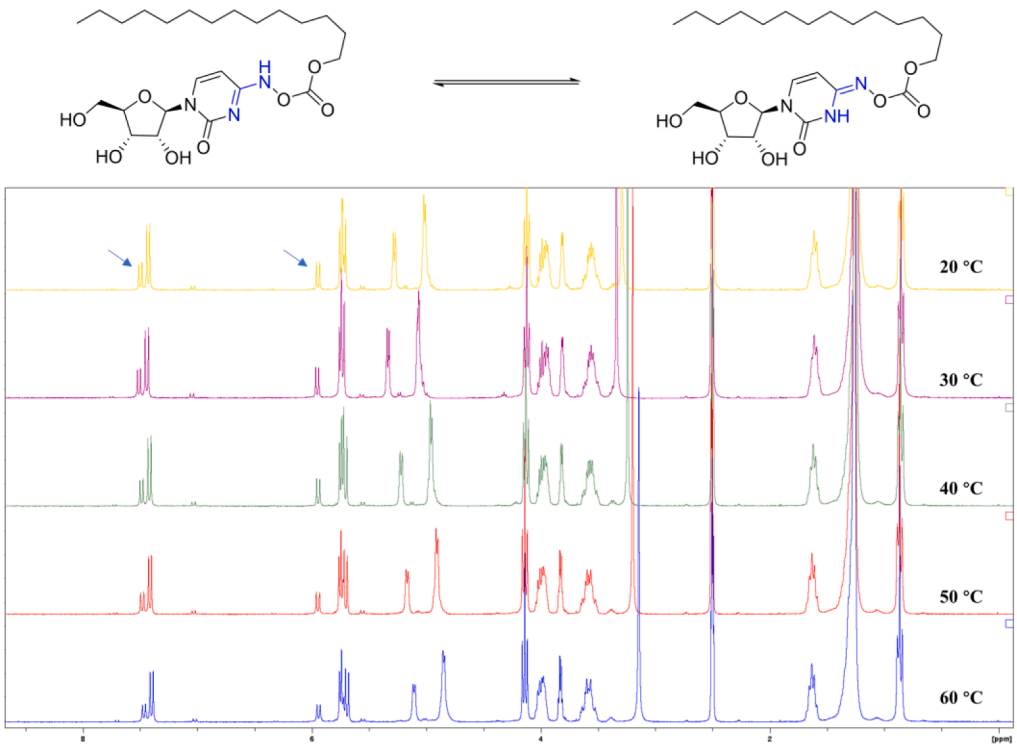

Fig. 2. Variable temperature (VT) NMR spectra of **2a** in DMSO-d_6. The arrow in spectra points to minor isomer peaks.

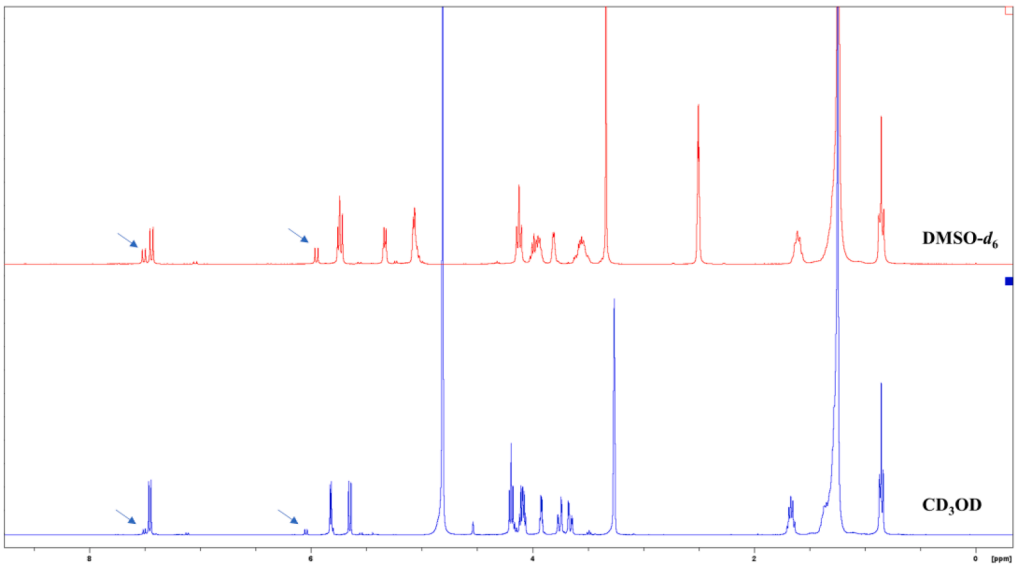

Fig. 3. ^{1}H NMR spectra of **2a** in DMSO-d_6 and CD_3OD. The arrow in spectra points to minor isomer peaks.

prodrugs in the infected cells [22–25]. This conjugation may result in the development of new prodrug forms of NHC having a longer duration of action by higher uptake into infected cells and sustained intracellular release of active substrates.

2.2. Synthesis of 3′-fluoro-NHC

3′-Fluoro-substituted nucleosides is an important class of nucleoside analogues that possess a broad-spectrum antiviral activity against diverse RNA and DNA viruses [31–33]. Here, the synthesis of 3′-deoxy-3′-fluoro modified NHC analogue **6** is shown in Scheme 2. The 3′-deoxy-3′-fluororibofuranosyl donor **3** was prepared starting from D-xylose following literature procedures [34–36]. The Vorbrüggen glycosylation with silylated benzoyl cytosine using trimethylsilyl trifluoromethanesulfonate (TMSOTf) as the Lewis acid at 85 °C in acetonitrile gave the nucleoside **4** in 43% yield. Deprotection of the benzoyl group with methanolic ammonia afforded nucleoside **5** in 77% yield. Finally, treatment of **5** with hydroxylamine sulfate to furnish target compound **6** in 62% yield.

2.3. Anti-SARS-CoV-2 activity

All of the lipid prodrugs **2a-d** and the 3′-deoxy-3′-fluoro modified NHC analogue **6** were evaluated for their activity against five different clinical isolates of SARS-CoV-2 (UC-1074, RG-2674, NVDBB-2220, 860-J1 and B1.1 529 BA.1) in Vero cells. The EC_{50} values of the synthesized compounds were calculated along with the determination of the effects on cell morphology and cell growth. NHC, molnupiravir and remdesivir were included as positive controls. The obtained results were summarized in Table 1.

As expected, the control drugs NHC, molnupiravir and remdesivir were endowed with potent antiviral activity against all the tested SARS-CoV-2 variants, especially, NHC, with EC_{50} values in the range of 0.28–0.89 μM. In general, lipid prodrugs **2a-d** potency (EC_{50} = 0.31–3.51 μM) was higher than that of molnupiravir (EC_{50} = 0.79–5.70 μM) and remdesivir (EC_{50} = 1.02–3.58 μM). Interestingly, all the prodrugs **2a-d** showed more potent antiviral activity against the Omicron variant (B1.1 529 BA.1) compared to other tested SARS-CoV-2 variants, with EC_{50} values in submicromolar concentrations (EC_{50} = 0.31–0.40 μM). The increased potency of **2a**, **2b**, and **2c** derivatives relative to molnupinavir was accompanied by an increase in the cytostatic activity of the compounds (CC_{50} = 4.03–6.32 μM), resulting in equal or lower

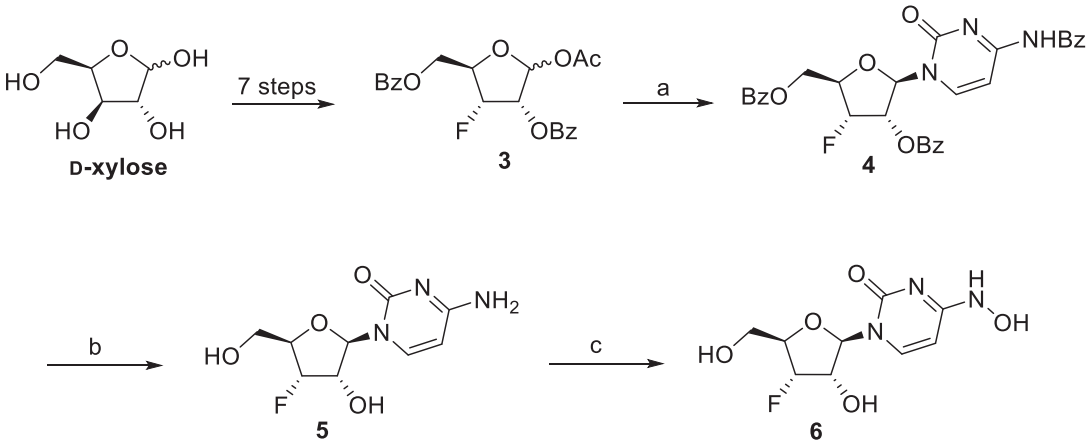

Scheme 2. Synthesis of 3′-fluoro-NHC. Reagents and conditions: (a) BSA, TMSOTf, MeCN, 80 °C, 6 h, 43%; (b) NH_3 in MeOH, rt, overnight, 77%; (c) $(NH_2OH)_2{\cdot}H_2SO_4$, 85 °C, 5 h, 62%.

Table 1
Antiviral activity and cytotoxicity of lipid prodrugs of NHC and 3′-F analogue of NHC against different SARS-CoV-2 variants in Vero cells.

Compound	Antiviral activity, EC_{50} (μM)[a]					cytotoxicity	
	UC-1074 (Wuhan)	RG-2674 (South African)	NVDBB-2220 (UK)	860-J1 (Delta)	B1.1 529 BA.1 (Omicron)	MCC[b]	CC_{50}[c]
2a	0.42	1.12	0.95	1.79	0.35	20	6.19
2b	0.42	0.89	1.13	2.51	0.31	≥20	6.32
2c	1.02	1.46	1.63	3.51	0.40	20	4.03
2d	0.41	1.51	1.12	2.08	0.33	≥20	16.33
6	>100	>100	>100	>100	29.91	≥100	ND[d]
NHC	0.30	0.48	0.53	0.89	0.28	20	5.47
Molnupiravir	4.00	5.70	3.98	5.43	0.79	≥60.7	39.32
Remdesivir	2.62	1.48	1.41	3.58	1.02	>40	>40

[a] Effective concentration required to reduce virus induced cytopathic effect by 50%. Virus input was 100 $TCID_{50}$ (The 50% Tissue Culture Infectious Dose).
[b] Minimum cytotoxic concentration that causes a microscopically detectable alteration of cell morphology.
[c] Cytostatic concentration required to reduce cell growth by 50%.
[d] Not determined. The results are mean of two independent experiments.

selectivity indices (ratio CC_{50}/EC_{50}) when compared to molnupinavir. Surprisingly, the lauroyl conjugate **2d** demonstrated the same selectivity as molnupinavir (selectivity indices in the range of 7–49). Although it was expected that fatty acyl conjugates with longer chain lengths might achieve a higher concentration of the prodrugs in the infected cells, no substantial increase in their activity against the tested SARS-CoV-2 variants and selectivity was found. The application of lipid prodrug strategy to NHC did not lead to a boost in antiviral activity, this could be due to the delayed release of the parent nucleoside in infected cells.

Unfortunately, the 3′-F analogue of NHC (**6**) only displayed minor activity against the Omicron variant (B1.1 529 BA.1), with an EC_{50} value of 29.91 μM, while completely devoid of activity against the Wuhan (UC-1074), South African (RG-2674), UK (NVDBB-2220) and Delta (860-J1) variants at the highest tested concentration (100 μM). The lack of antiviral activity of compound **6** indicates that NAs lack a 3′-hydroxyl group could not overcome SARS-CoV-2 exonuclease activity [37–39]. The results may offer invaluable insights for the development of more effective SARS-CoV-2 RdRp inhibitors.

2.4. Human plasma stability

To exert their antiviral activity, the lipid prodrugs should be stable in plasma and metabolized in the target cells to release intracellularly their parent nucleosides. Therefore, we determined the percentage digestion of molnupiravir and the lipid conjugates of NHC in human plasma and analysed the data using Liquid Chromatography Mass Spectrometry (LC-MS). Data are represented in the form of percentage degradation of test compounds against time by measuring peak area under the curve (Fig. 4). The carbonate prodrug **2a** was found to be labile in human plasma, only 17% of **2a** was observed at the 30 min time point, with a $t_{1/2}$ value about 10 min. However, the fatty acyl conjugates **2b-d** were found to be more stable, especially the palmitoyl conjugate **2b** and the myristyl conjugate **2c**, around 60% and 51% of the parent compound remained intact after 2 h incubation, respectively. Among all the tested prodrugs, the palmitoyl conjugate **2b** showed the best stability in human plasma with a $t_{1/2}$ value of 171 min, which was comparable to that of molnupiravir ($t_{1/2}$ = 187 min). The relative stability of prodrug **2b** clearly indicate that the lipid prodrugs of NHC could serve as promising leads for further optimization and development.

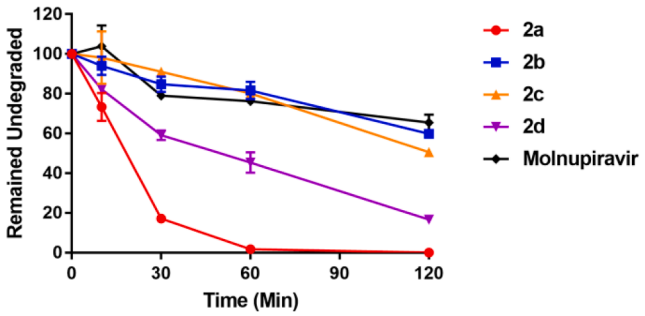

Fig. 4. Human plasma stability of **2a-d** and molnupiravir.

3. Conclusion

In summary, a series of lipid prodrugs of NHC and a 3′-fluorinated congener of NHC were synthesized, and tested for their anti-SARS-CoV-2 activity. All lipid prodrugs were endowed with interesting antiviral activity against all the tested SARS-CoV-2 variants, whereas the 3′-F modified analogue only showed minor antiviral activity against the SARS-CoV-2 omicron variant. The application of lipid prodrug strategy to NHC did not lead to a boost in antiviral potency, but the lipid prodrug **2d** of NHC displayed potent anti-SARS-CoV-2 activity with a selectivity comparable to that of the isopropyl prodrug molnupiravir. The in vitro plasma stability study showed that the palmitoyl conjugate **2b** exhibited comparable stability to that of molnupiravir. Overall, these data together indicate that the fatty acyl prodrugs of NHC deserve further investigation as new anti-SARS-CoV-2 agents.

4. Experimental section

4.1. Chemistry

Common solvents and reagents were purchased from commercial sources and were used as obtained. Magnetic resonance spectra (^{1}H NMR, ^{13}C NMR, and ^{19}F NMR) were measured with either a Bruker-400 or 600 MHz spectrometer. ^{1}H NMR chemical shifts are expressed in parts per million (δ) downfield from tetramethylsilane (DMSO-d_6 standardized at 2.50 ppm and CD_3OD standardized at 3.31 ppm). ^{13}C NMR chemical shifts are expressed in parts per million (δ) downfield from tetramethylsilane (central peak of DMSO-d_6 standardized at 39.52 ppm). ESI-MS spectra data were obtained using an API 4000 instrument. High-resolution mass spectrometry (HRMS) data were acquired by an AB_TripleTOF 5600 instrument. Reaction progress was monitored by thin layer chromatography (TLC) using silica gel GF254 plates, and spots were detected under UV light (254 and 366 nm). Compounds were purified by column chromatography using silica gel (200–300 mesh). Purities of all of the tested compounds were confirmed above 95% by using a Shimadzu analytical HPLC system on a C8 column (Inertsil Agilent ZORBAX Eclipse XDB-C8, 5 μm, 4.6 mm × 150 mm) using a gradient system (water/methanol) as a constant flow rate of 1 mL/min with UV detection at 254 nm.

4.1.1. General procedure for the synthesis of lipid prodrugs *2a-d*

To a solution of NHC (200 mg, 0.77 mmol) in anhydrous pyridine (4 mL) at 0 °C was added acid chloride (**1a-d**, 1.1 equiv, 0.85 mmol) dropwise. The reaction mixture was stirred at room temperature

overnight. Upon completing the reaction, the reaction mixture was concentrated under reduced pressure, and the residue was purified by silica gel column chromatography using a gradient of dichloromethane/methanol to give the target prodrugs **2a-d**.

4.1.2. 1-((2R,3R,4S,5R)-3,4-dihydroxy-5-(hydroxymethyl) tetrahydrofuran-2-yl)-4-((((tetradecyloxy)carbonyl)oxy)amino)pyrimidin-2(1H)-one (2a)

Compound **2a** was obtained from NHC and tetradecyl carbonochloridate (**1a**) in 77% yield as a white solid. NMR analysis shows a 7:3 mixture of rotamers. ^{1}H NMR (400 MHz, DMSO-d_6) δ 10.81 (s, 1H), 7.44 (d, J = 8.2 Hz, 1H), 5.95 (d, J = 8.2 Hz, 1H), 5.75 (d, J = 5.9 Hz, 1H), 5.32 (d, J = 4.5 Hz, 1H), 5.10–5.00 (m, 2H), 4.12 (t, J = 6.6 Hz, 2H), 4.02–3.91 (m, 2H), 3.81 (q, J = 3.2 Hz, 2H), 3.62–3.49 (m, 2H), 1.66–1.55 (m, 2H), 1.37–1.17 (m, 22H), 0.85 (t, J = 6.6 Hz, 3H). ^{1}H NMR (400 MHz, CD_3OD) δ 7.50 (d, J = 8.2 Hz, 1H), 5.87 (d, J = 5.0 Hz, 1H), 5.70 (d, J = 8.2 Hz, 1H), 4.24 (t, J = 6.6 Hz, 2H), 4.17–4.11 (m, 2H), 3.97 (q, J = 3.3 Hz, 1H), 3.82–3.69 (m, 2H), 1.75–1.68 (m, 2H), 1.40–1.23 (m, 22H), 0.85 (t, J = 6.6 Hz, 3H). ^{13}C NMR (100 MHz, DMSO-d_6) δ 153.62, 150.39, 149.28, 137.37, 134.93, 96.24, 87.68, 85.26, 73.47, 70.59, 68.37, 61.54, 31.77, 29.53, 29.51, 29.49, 29.46, 29.42, 29.19, 29.11, 28.65, 25.61, 22.57, 14.42. HRMS (ESI) calcd. for $C_{24}H_{42}N_3O_8$ $[M + H]^+$: 500.2966, found: 500.2970.

4.1.3. 1-((2R,3R,4S,5R)-3,4-dihydroxy-5-(hydroxymethyl) tetrahydrofuran-2-yl)-4-((palmitoyloxy)amino)pyrimidin-2(1H)-one (2b)

Compound **2b** was obtained from NHC and hexadecanoyl chloride (**1b**) in 62% yield as a white solid. NMR analysis shows a 5:1 mixture of rotamers. ^{1}H NMR (600 MHz, DMSO-d_6) δ 10.83 (s, 1H), 7.42 (d, J = 8.2 Hz, 1H), 5.76 (d, J = 5.9 Hz, 1H), 5.72 (d, J = 8.1 Hz, 1H), 5.31 (d, J = 6.0 Hz, 1H), 5.07–5.02 (m, 2H), 4.02–3.92 (m, 2H), 3.81 (q, J = 3.3 Hz, 1H), 3.62–3.50 (m, 2H), 2.43 (t, J = 7.5 Hz, 2H), 1.56–1.50 (m, 2H), 1.30–1.19 (m, 24H), 0.85 (t, J = 6.9 Hz, 3H). ^{1}H NMR (400 MHz, CD_3OD) δ 7.50 (d, J = 8.2 Hz, 1H), 5.88 (d, J = 5.1 Hz, 1H), 5.71 (d, J = 8.3 Hz, 1H), 4.17–4.11 (m, 2H), 3.97 (q, J = 3.3 Hz, 1H), 3.82–3.69 (m, 2H), 2.50 (t, J = 7.4 Hz, 2H), 1.56–1.50 (m, 2H), 1.41–1.22 (m, 24H), 0.90 (t, J = 6.7 Hz, 3H). ^{13}C NMR (150 MHz, DMSO-d_6) δ 170.67, 149.98, 149.63, 134.71, 96.73, 87.71, 85.26, 73.45, 70.60, 61.58, 32.41, 31.75, 29.50, 29.48, 29.46, 29.45, 29.37, 29.16, 29.14, 29.02, 28.96, 24.95, 24.88, 22.54, 14.37. HRMS (ESI) calcd. for $C_{25}H_{44}N_3O_7$ $[M + H]^+$: 498.3174, found: 498.3177.

4.1.4. 1-((2R,3R,4S,5R)-3,4-dihydroxy-5-(hydroxymethyl) tetrahydrofuran-2-yl)-4-((tetradecanoyloxy)amino)pyrimidin-2(1H)-one (2c)

Compound **2c** was obtained from NHC and myristoyl chloride (**1c**) in 82% yield as a white solid. NMR analysis shows a 5:1 mixture of rotamers. ^{1}H NMR (600 MHz, DMSO-d_6) δ 10.85 (s, 1H), 7.43 (d, J = 8.2 Hz, 1H), 5.77 (d, J = 5.9 Hz, 1H), 5.73 (d, J = 8.2 Hz, 1H), 5.32 (d, J = 5.8 Hz, 1H), 5.08–5.04 (m, 2H), 4.02–3.93 (m, 2H), 3.82 (q, J = 3.3 Hz, 1H), 3.62–3.51 (m, 2H), 2.44 (t, J = 7.5 Hz, 2H), 1.59–1.51 (m, 2H), 1.32–1.20 (m, 20H), 0.86 (t, J = 6.9 Hz, 3H). ^{13}C NMR (150 MHz, DMSO-d_6) δ 170.69, 149.98, 149.63, 134.71, 96.73, 87.71, 85.26, 73.45, 70.60, 61.58, 32.40, 31.75, 29.51, 29.48, 29.47, 29.45, 29.37, 29.16, 29.13, 29.00, 24.88, 22.54, 14.38. HRMS (ESI) calcd. for $C_{23}H_{40}N_3O_7$ $[M + H]^+$: 470.2861, found: 470.2861.

4.1.5. 1-((2R,3R,4S,5R)-3,4-dihydroxy-5-(hydroxymethyl) tetrahydrofuran-2-yl)-4-((dodecanoyloxy)amino)pyrimidin-2(1H)-one (2d)

Compound **2d** was obtained from NHC and lauroyl chloride (**1d**) in 82% yield as a white solid. NMR analysis shows a 5:1 mixture of rotamers. ^{1}H NMR (400 MHz, DMSO-d_6) δ 10.83 (s, 1H), 7.42 (d, J = 8.2 Hz, 1H), 5.76 (d, J = 5.8 Hz, 1H), 5.72 (d, J = 8.3 Hz, 1H), 5.32 (d, J = 5.6 Hz, 1H), 5.09–5.03 (m, 2H), 4.03–3.92 (m, 2H), 3.81 (q, J = 3.4 Hz, 1H), 3.63–3.49 (m, 2H), 2.43 (t, J = 7.4 Hz, 2H), 1.59–1.49 (m, 2H), 1.31–1.21 (m, 16H), 0.85 (t, J = 6.6 Hz, 3H). ^{13}C NMR (100 MHz, DMSO-d_6) δ 170.70, 149.98, 149.65, 134.70, 96.74, 87.60, 85.25, 73.45, 70.60, 61.56, 32.37, 31.77, 29.47, 29.39, 29.19, 29.14, 29.01, 24.94, 24.88, 22.57, 14.41. HRMS (ESI) calcd. for $C_{21}H_{36}N_3O_7$ $[M + H]^+$: 442.2548, found: 442.2549.

4.1.6. ((2R,3R,4S,5R)-5-(4-benzamido-2-oxopyrimidin-1(2H)-yl)-4-(benzoyloxy)-3-fluorotetrahydrofuran-2-yl)methyl benzoate (4)

A suspension of **3** (100 mg, 0.25 mmol) and N^4-Benzoylcytosine (160 mg, 0.75 mmol) in anhydrous CH_3CN (2 mL) was treated with BSA (0.40 mL, 1.49 mmol) and heated to 85 °C. Stirring and heating was continued until a clear solution was formed, and TMSOTf (0.16 mL, 1.49 mmol) was added. After heating at 80 °C for 6 h, the mixture was cooled to room temperature and quenched by the addition of sat. aq. $NaHCO_3$ solution (5 mL). The solution was then filtered and the filtrate was extracted by CH_2Cl_2. The combined organic phases were dried over anhydrous Na_2SO_4, filtered, and concentrated in vacuo. The residue was purified by silica gel column chromatography (petroleum ether/EtOAc, 1:1) to give **4** (60 mg, 43%) as a white solid. ^{1}H NMR (600 MHz, DMSO-d_6) δ 11.34 (s, 1H), 8.25 (d, J = 7.4 Hz, 1H), 8.07–7.48 (m, 15H), 7.34 (d, J = 7.6 Hz, 1H), 6.31 (d, J = 4.9 Hz, 1H), 5.94–5.87 (m, 1H), 5.71 (dt, J = 53.1, 4.8 Hz, 1H), 4.78 (dq, J = 22.2, 4.4 Hz, 1H), 4.72 (dd, J = 12.1, 3.7 Hz, 1H), 4.67 (dd, J = 12.1, 5.3 Hz, 1H). ^{13}C NMR (150 MHz, DMSO-d_6) δ 167.84, 165.96, 165.11, 164.25, 154.85, 146.89, 134.44, 134.06, 133.51, 133.25, 130.04, 129.82, 129.72, 129.35, 129.26, 129.07, 128.97, 128.89, 97.34, 90.00, 89.61 (d, $J_{C,F}$ = 189.2 Hz), 80.58 (d, $J_{C,F}$ = 25.3 Hz), 74.17 (d, $J_{C,F}$ = 13.7 Hz), 63.93 (d, $J_{C,F}$ = 6.2 Hz). ^{19}F NMR (471 MHz, DMSO-d_6) δ −201.10. MS (ESI) calcd. for $C_{30}H_{23}FN_3O_7$ $[M-H]^-$: 556.53, found: 555.91.

4.1.7. 4-amino-1-((2R,3S,4S,5R)-4-fluoro-3-hydroxy-5-(hydroxymethyl) tetrahydrofuran-2-yl)pyrimidin-2(1H)-one (5)

To a solution of **4** (250 mg, 0.45 mmol) in MeOH (1 mL) was added methanolic ammonia (7 N, 0.5 mL), and the mixture was stirred at room temperature overnight. The reaction mixture was concentrated under reduced pressure, and the residue was purified by silica gel column chromatography (CH_2Cl_2/MeOH, 10:1) to give **5** (85 mg, 77%) as a white solid. ^{1}H NMR (600 MHz, DMSO-d_6) δ 7.74 (d, J = 7.4 Hz, 1H), 7.24 (d, J = 19.3 Hz, 2H), 5.93 (d, J = 7.8 Hz, 1H), 5.73 (dd, J = 29.7, 6.9 Hz, 2H), 5.21 (t, J = 5.2 Hz, 1H), 4.92 (ddd, J = 54.8, 4.4, 1.3 Hz, 1H), 4.32–4.20 (m, 1H), 4.16–4.08 (m, 1H), 3.61–3.51 (m, 2H). ^{13}C NMR (150 MHz, DMSO-d_6) δ 166.01, 156.02, 142.04, 95.12, 93.17 (d, $J_{C,F}$ = 181.9 Hz), 87.90, 83.04 (d, $J_{C,F}$ = 21.8 Hz), 72.55 (d, $J_{C,F}$ = 16.0 Hz), 61.28 (d, $J_{C,F}$ = 10.8 Hz). ^{19}F NMR (471 MHz, DMSO-d_6) δ −197.31. MS (ESI) calcd. for $C_{18}H_{24}F_2N_6O_8Na$ $[2\ M + Na]^+$: 513.42, found: 512.77.

4.1.8. 1-((2R,3S,4S,5R)-4-fluoro-3-hydroxy-5-(hydroxymethyl) tetrahydrofuran-2-yl)-4-(hydroxyamino)pyrimidin-2(1H)-one (6)

To a solution of **5** (60 mg, 0.24 mmol) in H_2O (0.5 mL) was added hydroxylamine sulfate (60 mg, 0.36 mmol), and the mixture was stirred at 85 °C for 5 h. The reaction mixture was concentrated under reduced pressure, and the residue was purified by silica gel column chromatography (CH_2Cl_2/MeOH, 20:1) to give **6** (40 mg, 62%) as a white solid. NMR analysis shows a 13:1 mixture of rotamers. ^{1}H NMR (600 MHz, DMSO-d_6) δ 10.03 (s, 1H), 9.55 (s, 1H), 7.04 (d, J = 8.3 Hz, 1H), 5.82 (d, J = 8.3 Hz, 1H), 5.76 (d, J = 6.4 Hz, 1H), 5.62 (dd, J = 8.2, 1.6 Hz, 1H), 5.21 (t, J = 5.1 Hz, 1H), 4.90 (dd, J = 54.9, 4.3 Hz, 1H), 4.24–4.15 (m, 1H), 4.10 (dt, J = 28.3, 3.6 Hz, 1H), 3.62–3.57 (m, 1H), 3.55–3.49 (m, 1H). ^{13}C NMR (150 MHz, DMSO-d_6) δ 150.15, 143.73, 130.02, 99.46, 93.38 (d, $J_{C,F}$ = 181.3 Hz), 85.77, 82.91 (d, $J_{C,F}$ = 21.5 Hz), 71.32 (d, $J_{C,F}$ = 16.1 Hz), 61.30 (d, $J_{C,F}$ = 11.6 Hz). ^{19}F NMR (471 MHz, DMSO-d_6) δ −195.94. HRMS (ESI) calcd. for $C_9H_{13}FN_3O_5$ $[M + H]^+$: 262.0839, found: 262.0836.

4.2. SARS-CoV-2 antiviral assay

Vero cells (ATCC-CCL81) was used to evaluate the activity of the different compounds against SARS-CoV-2. Cells were grown in Dulbecco's Modified Eagle's Medium (DMEM, ThermoFisher, Belgium) supplemented with 10% fetal bovine serum (FBS), 2 mM L-glutamine, 0.1 mM non-essential amino acids, 1 mM sodium pyruvate and 10 mM HEPES at 37 °C in a 5% CO_2 humidified atmosphere. The SARS-CoV-2 variant, denoted UC-1074 was isolated in Vero cells (ATCC-CCL81) in 2020 from a nasopharyngeal swab of a COVID-19 patient who had a Ct of 19 for detection of SARS-CoV-2 E protein by RT-qPCR real-time reverse transcription PCR (RT-qPCR). The UC-1074 shares the same genome sequence as the early lineage A sequences (Wuhan/WH04/2020). Four variants of concern, kindly provided by Piet Maes (Laboratory of Clinical and Epidemiological Virology, Rega Institute, KU Leuven, Belgium) were used: NVDBB-2220 (Alpha variant), RG-2674 (Beta variant), 860-J1 (Delta variant) and B1.1.529 BA.1 (Omicron). All variants were used after 2–3 passages in cell culture. The infectious virus titer of the different variants was determined in Vero cells and expressed as 50% tissue culture infectious dose ($TCID_{50}$) per ml.

The cytopathic effect (CPE) reduction assay was used to evaluate the anti-SARS-CoV-2 activity of the compounds. Vero cells were seeded in 96-well plates at a density of $5x10^4$ cells per well in DMEM 10% FBS medium. After 4–5 days of growth, the cell culture medium was removed from the Vero cells grown to confluence, and cells were treated with 5-fold serial dilutions of the compounds diluted in fresh medium (DMEM 2% FBS) and were then mocked-infected or infected with 100 $TCID_{50}$/well of the SARS-CoV-2 variants (final volume 200 μL/ well). The starting drug concentrations of the compounds was 100 μM. Remdisivir, β-D-N^4-hydroxycytidine (NHC; EIDD-1931) and molnupiravir were used as reference anti-SARS-CoV-2 compounds. After 6–7 days of incubation at 35 °C, viral CPE was recorded microscopically based on detectable alterations of the cell morphology as soon as it reached completion in the untreated, virus-infected cells, using a 0 to 5 scale (with 0, being no CPE; 1, ~20% CPE; 2, 20 to 40% CPE; 3, ~40 to 60% CPE; 4, 60 to 80%; and 5, 80 to 100% CPE). The 50% effective concentration (EC_{50}), defined as the drug concentration that reduced the CPE by 50% compared to the untreated controls, was calculated for each compound from a non-linear curve fit using Prism 4.0b software.

In parallel, the cytotoxic effects of the derivatives were assessed by evaluating the MCC (minimum cytotoxic concentration that causes a microscopically detectable alteration of cell morphology). The effects of the compounds on cell growth were as well determined by counting the number of cells with a Coulter counter in mock-infected cultures and expressed as the cytostatic concentration required to reduce cell growth by 50% (CC_{50}). All SARS-CoV-2-related work was conducted in the BSL3 facilities of the KU Leuven Rega Institute (3CAPS) under licenses AMV 30112018 SBB 219 2018 0892 and AMV 23102017 SBB 219 2017 0589 according to institutional guidelines.

4.3. Plasma stability study

Human plasma stability assay was contracted and carried out by WuXi AppTec. The pooled frozen human plasma (3 male & 3 female from BioreclamationIVT, cat. #HUMANPLK2P2N, batch HMN708968) was thawed in a water bath at 37 °C prior to the experiment. Plasma was centrifuged at 4000 rpm for 5 min and the clots were removed if any. Using an Apricot automation workstation, plasma (98 μL/well) was added to a 96-well plate. The reaction was initiated by adding the test compounds to make a final concentration of 2 μM. Samples were then incubated at 37 °C and time points were taken at 0, 10, 30, 60, and 120 min. Time point samples were mixed with a quench solution containing internal standards tolbutamide (200 ng/mL) and labetalol (200 ng/mL) in MeCN. Quenched samples were centrifuged at 4000 rpm for 20 min at 4 °C. After centrifugation, each supernatant was transferred to a bioanalysis plate, followed by LC-MS/MS analysis.

Funding

This work was supported by the National Natural Science Foundation of China (82204199), the Natural Science Foundation of Shandong Province (ZR2021QB173), the High-end Foreign Experts Recruitment Program (G2021023002L), and the Young Scholars Program of Shandong University.

Declaration of Competing Interest

The authors declare that they have no known competing financial interests or personal relationships that could have appeared to influence the work reported in this paper.

Data availability

Data will be made available on request.

Acknowledgments

The authors thank Brecht Dirix for excellent technical assistance in the biological assays.

Appendix A. Supplementary material

Supplementary data to this article can be found online at https://doi.org/10.1016/j.bioorg.2023.106527.

References

[1] https://covid19.who.int/.
[2] G. Li, E. De Clercq, Therapeutic options for the 2019 novel coronavirus (2019-nCoV), Nat. Rev. Drug Discov. 19 (3) (2020) 149–150.
[3] C. Gil, T. Ginex, I. Maestro, V. Nozal, L. Barrado-Gil, M.A. Cuesta-Geijo, J. Urquiza, D. Ramirez, C. Alonso, N.E. Campillo, A. Martinez, COVID-19: drug targets and potential treatments, J. Med. Chem. 63 (21) (2020) 12359–12386.
[4] D.L. McKee, A. Sternberg, U. Stange, S. Laufer, C. Naujokat, Candidate drugs against SARS-CoV-2 and COVID-19, Pharmacol. Res. 157 (2020), 104859.
[5] A. Shannon, B. Canard, Kill or corrupt: Mechanisms of action and drug-resistance of nucleotide analogues against SARS-CoV-2, Antiviral Res. 210 (2023), 105501.
[6] J.H. Beigel, K.M. Tomashek, L.E. Dodd, A.K. Mehta, B.S. Zingman, A.C. Kalil, E. Hohmann, H.Y. Chu, A. Luetkemeyer, S. Kline, D. Lopez de Castilla, R. W. Finberg, K. Dierberg, V. Tapson, L. Hsieh, T.F. Patterson, R. Paredes, D. A. Sweeney, W.R. Short, G. Touloumi, D.C. Lye, N. Ohmagari, M.D. Oh, G.M. Ruiz-Palacios, T. Benfield, G. Fatkenheuer, M.G. Kortepeter, R.L. Atmar, C.B. Creech, J. Lundgren, A.G. Babiker, S. Pett, J.D. Neaton, T.H. Burgess, T. Bonnett, M. Green, M. Makowski, A. Osinusi, S. Nayak, H.C. Lane, A.-S.-G. Members, Remdesivir for the treatment of Covid-19 - final report, N. Engl. J. Med. 383 (19) (2020) 1813–1826.
[7] Z. Cao, W. Gao, H. Bao, H. Feng, S. Mei, P. Chen, Y. Gao, Z. Cui, Q. Zhang, X. Meng, H. Gui, W. Wang, Y. Jiang, Z. Song, Y. Shi, J. Sun, Y. Zhang, Q. Xie, Y. Xu, G. Ning, Y. Gao, R. Zhao, VV116 versus nirmatrelvir-ritonavir for oral treatment of Covid-19, N. Engl. J. Med. 388 (5) (2023) 406–417.
[8] Z. Ren, H. Luo, Z. Yu, J. Song, L. Liang, L. Wang, H. Wang, G. Cui, Y. Liu, J. Wang, Q. Li, Z. Zeng, S. Yang, G. Pei, Y. Zhu, W. Song, W. Yu, C. Song, L. Dong, C. Hu, J. Du, J. Chang, A. Randomized, Open-label, controlled clinical trial of azvudine tablets in the treatment of mild and common COVID-19, a pilot study, Adv. Sci. 7 (19) (2020) e2001435.
[9] S.S. Good, J. Westover, K.H. Jung, X.J. Zhou, A. Moussa, P. La Colla, G. Collu, B. Canard, J.P. Sommadossi, AT-527, a double prodrug of a guanosine nucleotide analog, is a potent inhibitor of SARS-CoV-2 in vitro and a promising oral antiviral for treatment of COVID-19, Antimicrob. Agents Chemother. 65 (4) (2021) e02479–e2520.
[10] R.T. Eastman, J.S. Roth, K.R. Brimacombe, A. Simeonov, M. Shen, S. Patnaik, M. D. Hall, Remdesivir: a review of its discovery and development leading to emergency use authorization for treatment of COVID-19, ACS Cent. Sci. 6 (5) (2020) 672–683.
[11] W.A. Fischer, J.J. Eron, W. Holman, M.S. Cohen, L. Fang, L.J. Szewczyk, T. P. Sheahan, R. Baric, K.R. Mollan, C.R. Wolfe, E.R. Duke, M.M. Azizad, K. Borroto-Esoda, D.A. Wohl, R.W. Coombs, A.J. Loftis, P. Alabanza, F. Lipansky, W.P. Painter, A phase 2a clinical trial of molnupiravir in patients with COVID-19 shows accelerated SARS-CoV-2 RNA clearance and elimination of infectious virus, Sci. Transl. Med. 14 (628) (2022) eabl7430.
[12] A.K. Singh, A. Singh, R. Singh, A. Misra, Molnupiravir in COVID-19: a systematic review of literature, Diabetes Metab. Syndr. 15 (6) (2021), 102329.
[13] A. Wahl, L.E. Gralinski, C.E. Johnson, W. Yao, M. Kovarova, K.H. Dinnon, H. Liu, V. J. Madden, H.M. Krzystek, C. De, K.K. White, K. Gully, A. Schäfer, T. Zaman, S. R. Leist, P.O. Grant, G.R. Bluemling, A.A. Kolykhalov, M.G. Natchus, F.B. Askin,

G. Painter, E.P. Browne, C.D. Jones, R.J. Pickles, R.S. Baric, J.V. Garcia, SARS-CoV-2 infection is effectively treated and prevented by EIDD-2801, Nature 591 (7850) (2021) 451–457.
[14] L. Tian, Z. Pang, M. Li, F. Lou, X. An, S. Zhu, L. Song, Y. Tong, H. Fan, J. Fan, Molnupiravir and its antiviral activity against COVID-19, Front. Immunol. 13 (2022), 855496.
[15] W.P. Painter, W. Holman, J.A. Bush, F. Almazedi, H. Malik, N. Eraut, M.J. Morin, L. J. Szewczyk, G.R. Painter, Human safety, tolerability, and pharmacokinetics of molnupiravir, a novel broad-spectrum oral antiviral agent with activity against SARS-CoV-2, Antimicrob. Agents Chemother. 65 (5) (2021) e02428–e2520.
[16] R.M. Cox, J.D. Wolf, R.K. Plemper, Therapeutically administered ribonucleoside analogue MK-4482/EIDD-2801 blocks SARS-CoV-2 transmission in ferrets, Nat. Microbiol. 6 (1) (2021) 11–18.
[17] S. Zhou, C.S. Hill, S. Sarkar, L.V. Tse, B.M.D. Woodburn, R.F. Schinazi, T. P. Sheahan, R.S. Baric, M.T. Heise, R. Swanstrom, β-d-N4-hydroxycytidine inhibits SARS-CoV-2 through lethal mutagenesis but is also mutagenic to mammalian cells, J. Infect. Dis. 224 (3) (2021) 415–419.
[18] M. Imran, M. Kumar Arora, S.M.B. Asdaq, S.A. Khan, S.I. Alaqel, M.K. Alshammari, M.M. Alshehri, A.S. Alshrari, A. Mateq Ali, A.M. Al-Shammeri, B.D. Alhazmi, A.A. Harshan, M.T. Alam, Abida, Discovery, Development, and Patent Trends on Molnupiravir: A Prospective Oral Treatment for COVID-19, Molecules 26(19) (2021) 5795.
[19] F. Kabinger, C. Stiller, J. Schmitzová, C. Dienemann, G. Kokic, H.S. Hillen, C. Höbartner, P. Cramer, Mechanism of molnupiravir-induced SARS-CoV-2 mutagenesis, Nat. Struct. Mol. Biol. 28 (9) (2021) 740–746.
[20] M.L. Agostini, A.J. Pruijssers, J.D. Chappell, J. Gribble, X. Lu, E.L. Andres, G. R. Bluemling, M.A. Lockwood, T.P. Sheahan, A.C. Sims, M.G. Natchus, M. Saindane, A.A. Kolykhalov, G.R. Painter, R.S. Baric, M.R. Denison, Small-molecule antiviral beta-d-N(4)-hydroxycytidine inhibits a proofreading-intact coronavirus with a high genetic barrier to resistance, J. Virol. 93 (24) (2019) e01348–e1419.
[21] J.J. Yoon, M. Toots, S. Lee, M.E. Lee, B. Ludeke, J.M. Luczo, K. Ganti, R.M. Cox, Z. M. Sticher, V. Edpuganti, D.G. Mitchell, M.A. Lockwood, A.A. Kolykhalov, A. L. Greninger, M.L. Moore, G.R. Painter, A.C. Lowen, S.M. Tompkins, R. Fearns, M. G. Natchus, R.K. Plemper, Orally efficacious broad-spectrum ribonucleoside analog inhibitor of influenza and respiratory syncytial viruses, Antimicrob. Agents Chemother. 62 (8) (2018) e00766–e818.
[22] H.K. Agarwal, B.S. Chhikara, M.J. Hanley, G.F. Ye, G.F. Doncel, K. Parang, Synthesis and biological evaluation of fatty acyl ester derivatives of (-)-2',3'-dideoxy-3'-thiacytidine, J. Med. Chem. 55 (10) (2012) 4861–4871.
[23] H.K. Agarwal, K. Loethan, D. Mandal, G.F. Doncel, K. Parang, Synthesis and biological evaluation of fatty acyl ester derivatives of 2',3'-didehydro-2',3'-dideoxythymidine, Bioorg. Med. Chem. Lett. 21 (7) (2011) 1917–1921.
[24] H.K. Agarwal, B.S. Chhikara, S. Bhavaraju, D. Mandal, G.F. Doncel, K. Parang, Emtricitabine prodrugs with improved anti-HIV activity and cellular uptake, Mol. Pharm. 10 (2) (2013) 467–476.
[25] N.S. El-Sayed, A.S. Jureka, M.R. Edwards, S. Lohan, C.G. Williams, P.T. Keiser, R. A. Davey, J. Totonchy, R.K. Tiwari, C.F. Basler, K. Parang, Synthesis and antiviral activity of fatty acyl conjugates of remdesivir against severe acute respiratory syndrome coronavirus 2 and Ebola virus, Eur. J. Med. Chem. 226 (2021), 113862.
[26] R.T. Schooley, A.F. Carlin, J.R. Beadle, N. Valiaeva, X.Q. Zhang, A.E. Clark, R. E. McMillan, S.L. Leibel, R.N. McVicar, J. Xie, A.F. Garretson, V.I. Smith, J. Murphy, K.Y. Hostetler, Rethinking remdesivir: synthesis, antiviral activity, and pharmacokinetics of oral lipid prodrugs, Antimicrob. Agents Chemother. 65 (10) (2021) e0115521.
[27] H. Hu, M.D. Mady Traore, R. Li, H. Yuan, M. He, B. Wen, W. Gao, C.B. Jonsson, E. A. Fitzpatrick, D. Sun, Optimization of the prodrug moiety of remdesivir to improve lung exposure/selectivity and enhance anti-SARS-CoV-2 activity, J. Med. Chem. 65 (18) (2022) 12044–12054.
[28] W. Painter, A. Robertson, L.C. Trost, S. Godkin, B. Lampert, G. Painter, First pharmacokinetic and safety study in humans of the novel lipid antiviral conjugate CMX001, a broad-spectrum oral drug active against double-stranded DNA viruses, Antimicrob. Agents Chemother. 56 (5) (2012) 2726–2734.
[29] D. Irby, C. Du, F. Li, Lipid-drug conjugate for enhancing drug delivery, Mol. Pharm. 14 (5) (2017) 1325–1338.
[30] D.J. Paymode, N. Vasudevan, S. Ahmad, A.L. Kadam, F.S.P. Cardoso, J.M. Burns, D. W. Cook, R.W. Stringham, D.R. Snead, Toward a practical, two-step process for molnupiravir: direct hydroxamination of cytidine followed by selective esterification, Org. Process Res. Dev. 25 (8) (2021) 1822–1830.
[31] A. Van Aerschot, P. Herdewijn, G. Janssen, M. Cools, E. De Clercq, Synthesis and antiviral activity evaluation of 3'-fluoro-3'-deoxyribonucleosides: broad-spectrum antiviral activity of 3'-fluoro-3'-deoxyadenosine, Antiviral Res. 12 (3) (1989) 133–150.
[32] I.A. Mikhailopulo, N.E. Poopeiko, T.I. Prikota, G.G. Sivets, E.I. Kvasyuk, J. Balzarini, E. De Clercq, Synthesis and antiviral and cytostatic properties of 3'-deoxy-3'-fluoro- and 2'-azido-3'-fluoro-2',3'-dideoxy-D-ribofuranosides of natural heterocyclic bases, J. Med. Chem. 34 (7) (1991) 2195–2202.
[33] L. Eyer, P. Svoboda, J. Balvan, T. Vicar, M. Raudenska, M. Stefanik, J. Haviernik, I. Huvarova, P. Strakova, I. Rudolf, Z. Hubalek, K. Seley-Radtke, E. de Clercq, D. Ruzek, Broad-spectrum antiviral activity of 3'-deoxy-3'-fluoroadenosine against emerging flaviviruses, Antimicrob. Agents Chemother. 65 (2) (2021) e01522–e1620.
[34] J. Bouton, A.F. d'Almeida, L. Maes, G. Caljon, S. Van Calenbergh, F. Hulpia, Synthesis and evaluation of 3'-fluorinated 7-deazapurine nucleosides as antikinetoplastid agents, Eur. J. Med. Chem. 216 (2021), 113290.
[35] I.A. Mikhailopulo, G.G. Sivets, A novel route for the synthesis of deoxy fluoro sugars and nucleosides, Helv. Chim. Acta 82 (11) (1999) 2052–2065.
[36] I.A. Mikhailopulo, G.G. Sivets, N.B. Khripach, A novel route for the synthesis of fluorodeoxy sugars and nucleosides, Nucleosides Nucleotides 18 (4–5) (1999) 689–690.
[37] F. Robson, K.S. Khan, T.K. Le, C. Paris, S. Demirbag, P. Barfuss, P. Rocchi, W.L. Ng, Coronavirus RNA proofreading: molecular basis and therapeutic targeting, Mol. Cell 80 (6) (2020) 1136–1138.
[38] N.H. Moeller, K. Shi, O. Demir, C. Belica, S. Banerjee, L.L. Yin, C. Durfee, R.E. Amaro, H. Aihara, Structure and dynamics of SARS-CoV-2 proofreading exoribonuclease ExoN, Proc. Natl. Acad. Sci. U. S. A. 119(9) (2022) e2106379119.
[39] X.T. Wang, C.J. Tao, I. Morozova, S. Kalachikov, X.X. Li, S. Kumar, J.J. Russo, J. Y. Ju, Identifying structural features of nucleotide analogues to overcome SARS-CoV-2 exonuclease activity, Viruses 14 (7) (2022) 1413.